Journal of Molecular Liquids 335 (2021) 116136

Contents lists available at ScienceDirect

Journal of Molecular Liquids

journal homepage: www.elsevier.com/locate/molliq

Experimental and molecular dynamics study of graphene oxide quantum dots interaction with solvents and its aggregation mechanism

V.R. Jauja-Ccana [a,*], Allison V. Cordova-Huaman [a], Gustavo T. Feliciano [b], Adolfo La Rosa-Toro Gómez [a]

[a] Laboratorio de Investigación de Electroquímica Aplicada, Facultad de Ciencias, Universidad Nacional de Ingeniería, Av. Tupac Amaru 210, Rimac, Lima, Peru
[b] Institute of Chemistry, Department of Engineering, Physics and Mathematics, São Paulo State University (UNESP), 14800-060 Araraquara, São Paulo, Brazil

ARTICLE INFO

Article history:
Received 2 November 2020
Revised 15 March 2021
Accepted 8 April 2021
Available online 20 April 2021

Keywords:
Graphene oxide quantum dots
Aggregation
RDF
Face-to-face
π-π stacking

ABSTRACT

This work describes the aggregation process and explains the optical behavior of graphene oxide quantum dots (GOQDs) in different solvents using molecular dynamics, DFT, and experimental observations. The optical behavior of electrochemically synthesized GOQDs in different solvents was analyzed by UV–Vis spectroscopy, and dependence between the spectra and the solvents (water, ethanol, acetone, chloroform, toluene, and n-hexane) was found. Molecular dynamics methods were used to determine that the local structure of the solvent molecules and the nature of intermolecular forces between GOQDs dominate their aggregation state and their optical properties in each solvent. These computational studies based on liquid-liquid systems provide a fast and straightforward approach to develop synthesis and purification methods that allow tailored advanced optical properties of GOQDs.

1. Introduction

Graphene quantum dots (GQDs), members of the graphene family materials, have shown interesting optical and electronic properties since their discovery. These properties, along with their high chemical stability and biocompatibility, make GQDs suitable for a broad spectrum of applications such as photocatalysis [1], electrocatalysis [2], bioimage [3], sensors [4,5], photovoltaic solar cells [6] and so on. GQDs can be obtained from different methods, including top down [7] (chemical and electrochemical exfoliation, acidic oxidation [4], hydrotermal) and bottom-up [7] (microwave-assisted pyrolysis [3,8], electrochemical carbonization [5,9]) synthesis strategies.

Important features of GQDs, such as their behavior as metal-free semiconductor [9,10] and their optical properties, are related to their size (quantum confinement), shape [11], surface chemical composition (edge effect), functionalization with oxygenated groups (—OH, —COOH, C═O) [12–15] or doping with N, S, Se or B [16–18]. When an oxidative method is used for GQDs synthesis, these particles present a higher degree of functionalization with oxygenated groups. These groups are mainly located at the edge of the particles, increasing the reactivity in these positions. Due to the number of oxygenated functional groups, these types of particles receive the name of graphene oxide quantum dots (GOQDs) or oxygenated GQDs [12,13,15].

Applications based on GOQDs include chemical sensors [19], electrocatalysis [20], biomedical [21], and others. However, despite the significant number of synthesis methods, these applications are limited because their purification and extraction demand a high cost in time and money [9]. Therefore, the identification of physical properties of GOQDs in different solvents, such as the adopted aggregation in them, could help identify solvents that can facilitate their extraction.

Several studies have reported that the optical properties of GOQDs vary depending on the solvent (negative solvatochromism) [22], and the aggregation state they adopt on it [23-25] As observed by Chinnusami et al [24] and Shixiong et al [26], GOQDs aggregates retard the charge transfer during photocatalytic processes, decreasing its efficiency. This effect gains interest under the consideration that GQDs and carbon quantum dots (CQDs) formed by pilled GQDs [27], generate very stable suspensions, and that these do not show signs of precipitation even after a year [27,28]. Therefore, the comprehension of the aggregation process of GQDs and GOQDs could help choose the ideal solvent for preparing GOQDs or CQDs composites, depending on the application.

Forces like π-π stacking, hydrogen bonds, van der Waals interactions, electrostatic interactions, and collision of solvent molecules dominate the aggregation of graphenic materials (polyaromatic molecules) [29]. Molecular dynamics (MD) methods offer several advantages to study the behavior of graphenic

* Corresponding author.
E-mail address: vjaujac@uni.pe (V.R. Jauja-Ccana).

https://doi.org/10.1016/j.molliq.2021.116136
0167-7322/

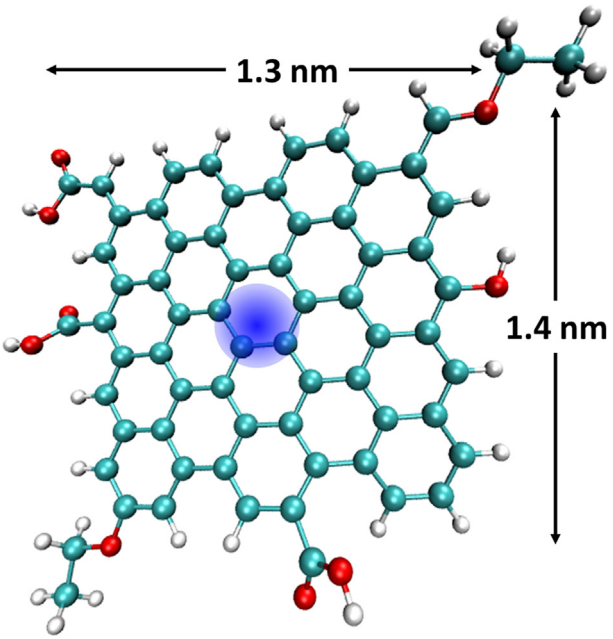

Fig. 1. Optimized structure of GOQDs according to B3LYP/6-311G(d,p) theory level. The blue circle shows the center of mass of the structure (COM).

materials in different solvents, such as graphene sheets [30], functionalized graphene sheets [31], fullerenes [32,33], carbon nanotubes [34], graphene oxide sheets [29], carbon dots[27] and other polyaromatic compounds, such as asphaltenes [35,36]. These methods allow the understanding of the adopted mechanism of GOQDs aggregation, which can be face-to-face (H aggregates), parallel-displaced (J aggregates), or T-shaped [36–38].

In this paper, we present results from MD simulations to understand the behavior of quantum dots of graphene oxide in polar (water, ethanol, and acetone), non-polar (chloroform and n-hexane), and aromatic (toluene) solvents. The aggregation state was evaluated by radial distribution functions (RDF), mean square displacement (MSD), and the number of hydrogen bonds (H-bond). These results are contrasted with experimental UV–Vis spectroscopy measurements of electrochemically synthesized GOQDs in different solvents.

2. Experimental and computational details

2.1. GOQDs synthesis

GOQDs were synthesized by an electrochemical carbonization method [5,9,39,40], using ethanol as a carbon source in an alkaline medium. Briefly, a mixture of ethanol (96%) and KOH 0.01 M was sonicated for 10 min. This was used as the electrolyte in a two-electrodes cell composed of two graphite rods (area of 2 cm^2). A constant potential of 10 V was applied for 4 h to this system. After this time, the initially transparent solution acquired a brown color.

2.2. UV–Vis absorption and FT-IR measurements

The UV–Vis spectroscopic measurements of GOQDs were performed in a UV-3150 spectrophotometer (Shimadzu, Kyoto, Japan) using quartz cells. The samples were prepared by pipetting an aliquot of a GOQDs dispersion in the chosen solvents (1:20) and sonicating them for 30 min. The mixture was then left at room temperature for 24 h for its stabilization. A blank sample of each

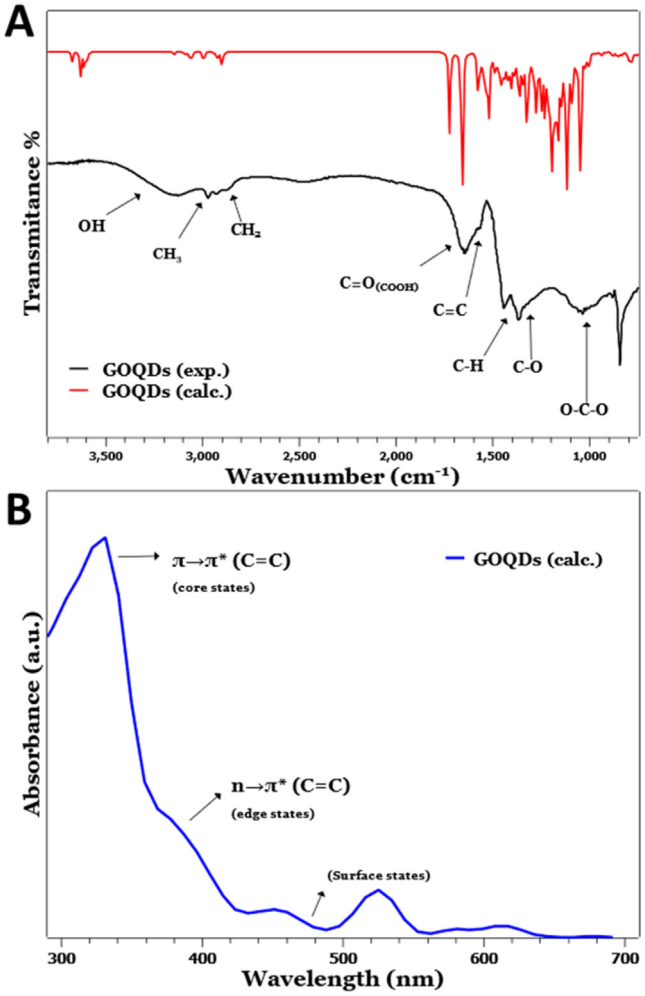

Fig. 2. (A) Calculated and experimental FTIR spectra of GOQDs and (B) calculated UV–Vis absorption spectrum using CAM-B3LYP/6-31G(d) theory level.

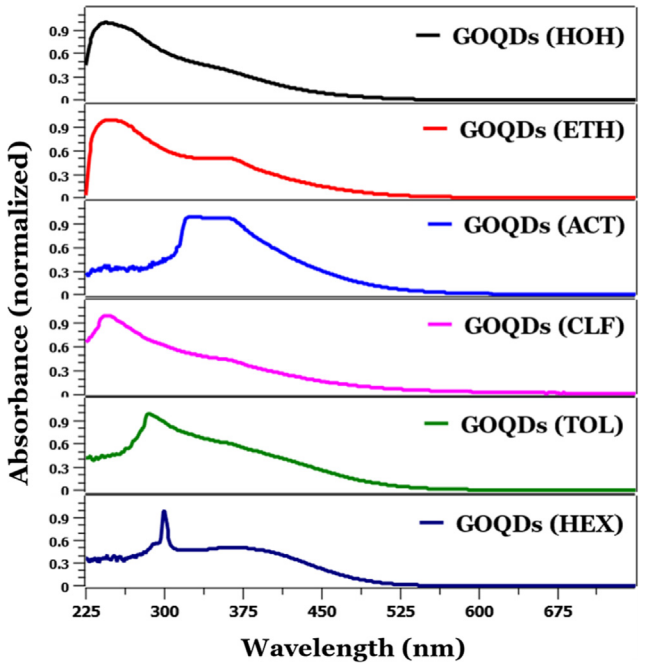

Fig. 3. Experimental UV–Vis spectra of GOQDs in different solvents (water, ethanol, acetone, chloroform, toluene, and n-hexane).

solvent was prepared similarly, adding ethanol and KOH without applying the oxidation potential.

The Fourier transform infrared (FT-IR) spectra were recorded using KBr pellets using a Perkin Elmer GX spectrophotometer over the range of 4000–400 cm^{-1} with a resolution of 1 cm^{-1}.

2.3. Computational details

The chemical structure of graphene oxide quantum dots (GOQDs) was constructed based on the pH effect [38], the typical outcome of a standard oxidation process [41], and experimental

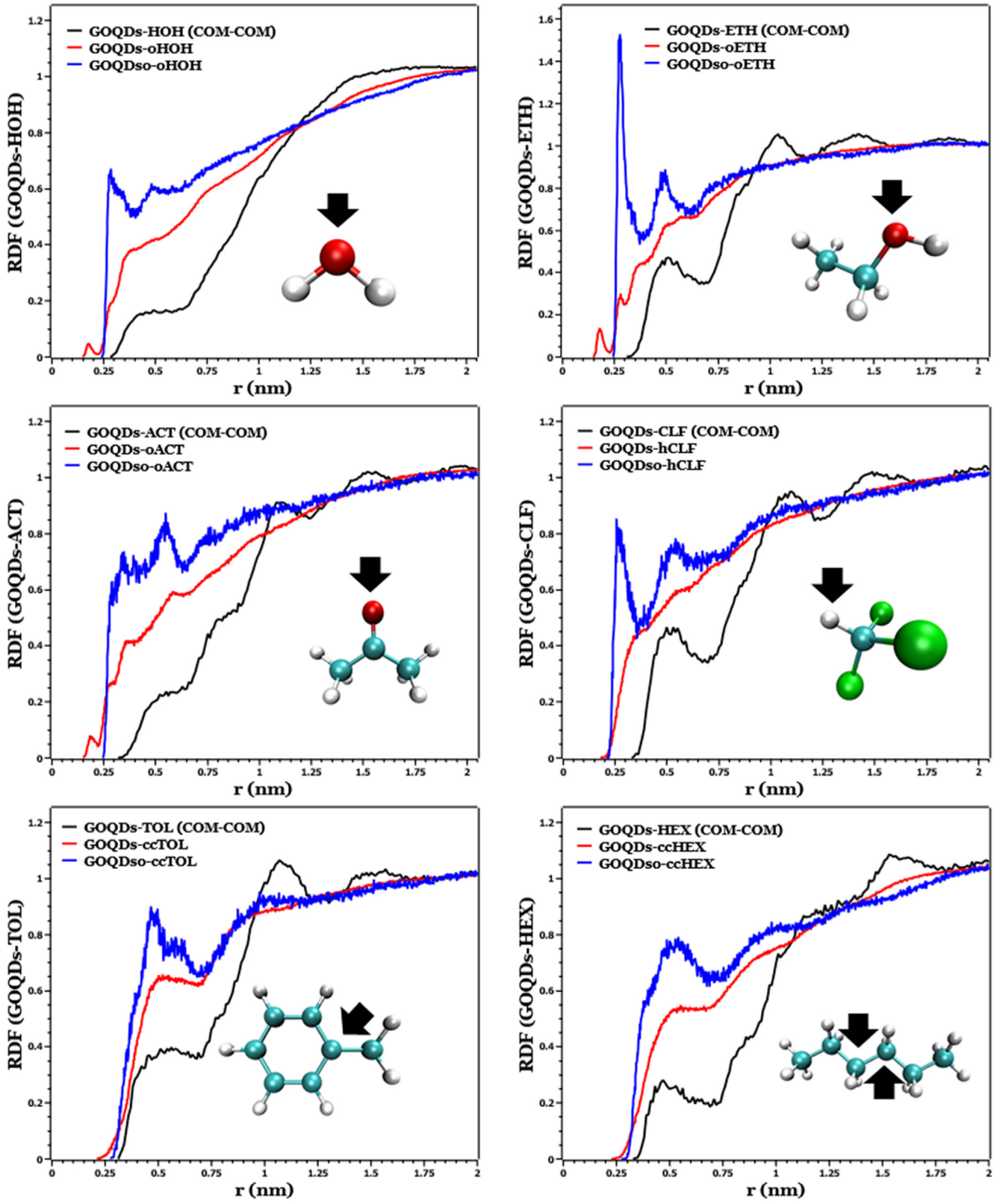

Fig. 4. RDF curves of solvent molecules around GOQDs after 5 ns (time of complete aggregation state of GOQDs in water).

results. This structure contains epoxy, hydroxyl, and carboxyl groups, as the FT-IR results suggest. The size of the GOQDs (1.4 n m × 1.3 nm) used in this study was chosen to represent the experimental size of GOQDS obtained by electrochemical methods (1–10 nm) [13,39,42,43] (Fig. 1). The optimization and vibrational frequency analysis of GOQDs, water (HOH), ethanol (ETH), acetone (ACT), chloroform (CLF), toluene (TOL), and n-hexane (HEX) structures were done using Gaussian 16 software at the B3LYP/6-311G (d,p) [44] theory level. UV–Vis spectra calculations of GOQDs and their aggregates (face-to-face, parallel displaced, and T-shape) were carried out using CAM-B3LYP/6-31G(d) level of theory without solvation. Atomic charges were evaluated using a corrected ADCH model with the MULTIWFN package [45].

Optimized potential for liquid simulation/all atoms (OPLS/AA) [46] force field was employed to to model molecules of water, acetone, ethanol, chloroform, toluene, n-hexane, and GOQDs with ethyl, hydroxyl, and carboxyl functional groups. The force field parameters of carbon atoms in GOQDs were taken from Patra and Zeng's work [47,48].

MD simulations were performed using the GROMACS 5.1 [49,50] package with periodic boundary conditions in all directions. Both van der Waals and Coulombic interactions were treated with a smooth cutoff at a distance of 10 Å. Visual Molecular Dynamics, VMD, was used for the simulation analysis [51].

The aggregation process of GOQDs in solvents was studied through standard MD simulations. To do this, four GOQDs particles and, subsequently, the solvent molecules were distributed randomly in a 5.0 nm cubic box (Fig. S1A and B). Energy minimization ensured a stable initial configuration. Before the simulation, the system was equilibrated in a canonical ensemble NVT at 298 K. The system was relaxed in an NPT ensemble at 298 K and atmospheric pressure. Radial distribution functions (RDF) were used to analyze the occurrence of aggregation

3. Results and discussion

3.1. Experimental and computational FT-IR and UV–Vis spectra

Calculated and experimental FT-IR spectra of the GOQDs are shown in Fig. 2.A. The FT-IR was computed at the B3LYP level using the triple split valence basis and the diffuse functions 6-311G(d, p). A scaling factor of 0.9661 was used on the calculated vibrational frequencies to compare it with experimental results. Stretching signals of —OH from —COOH groups appear as two bands (3820 cm^{-1} and 3180 cm^{-1}) in the calculated spectrum and as one in the experimental (between 3743 and 3774 cm^{-1}). The calculated signal at 3184 cm^{-1} relates to the stretching of —CH groups attached to the aromatic rings, which can also be seen at 2969 cm^{-1} in the experimental spectrum. —CH_2— and —CH_3 signals were observed experimentally around 2944–2848 cm^{-1} and were calculated at 2938–2853 cm^{-1} [3,8,52]. The calculated and experimental —CH bending vibrations from the ethoxide group were observed at 3016 cm^{-1} and 2927 cm^{-1}, respectively. The asymmetric O═COH stretching appears at 1725 cm^{-1} in the calculated spectrum and experimentally at 1682 cm^{-1}. The calculated bands at 1641 cm^{-1} and 1463 cm^{-1} relate to the C═C stretching and the —CH_2— bending. Their experimental values correspond to 1643 cm^{-1} and 1460 cm^{-1} bands [53,54]. Vibrational frequencies of —OH and —CH stretching were calculated at 1370 cm^{-1} [54], and observed at 1364 cm^{-1}. Finally, the strong, calculated band at 1044 cm^{-1} relates to the COC stretching, which is in good agreement with its corresponding experimental value at 1042 cm^{-1}.

Electronic transitions of GOQDs were studied from an optimized structure at B3LYP/6-311G(d, p) through a theoretical UV–Vis spectrum calculated using CAM-B3LYP/6-31G(d) in the gas phase (Fig. 2.B). The absorption spectrum of GOQDs exhibits three

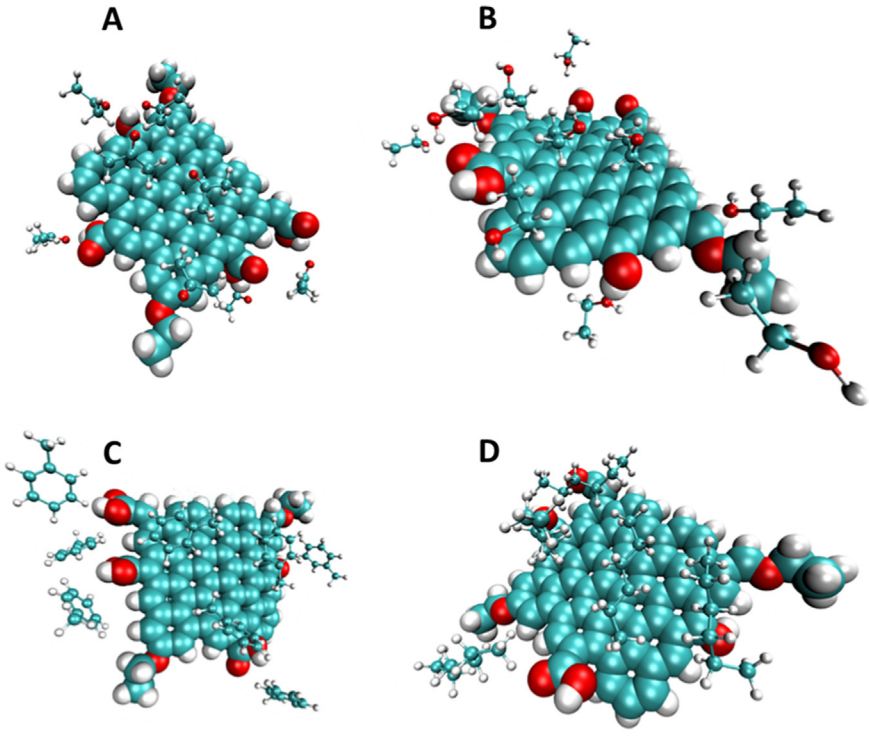

Fig. 5. Configuration of (A) acetone, (B) ethanol, (C) toluene, and (D) n-hexane around GOQDs after 5 ns of simulation.

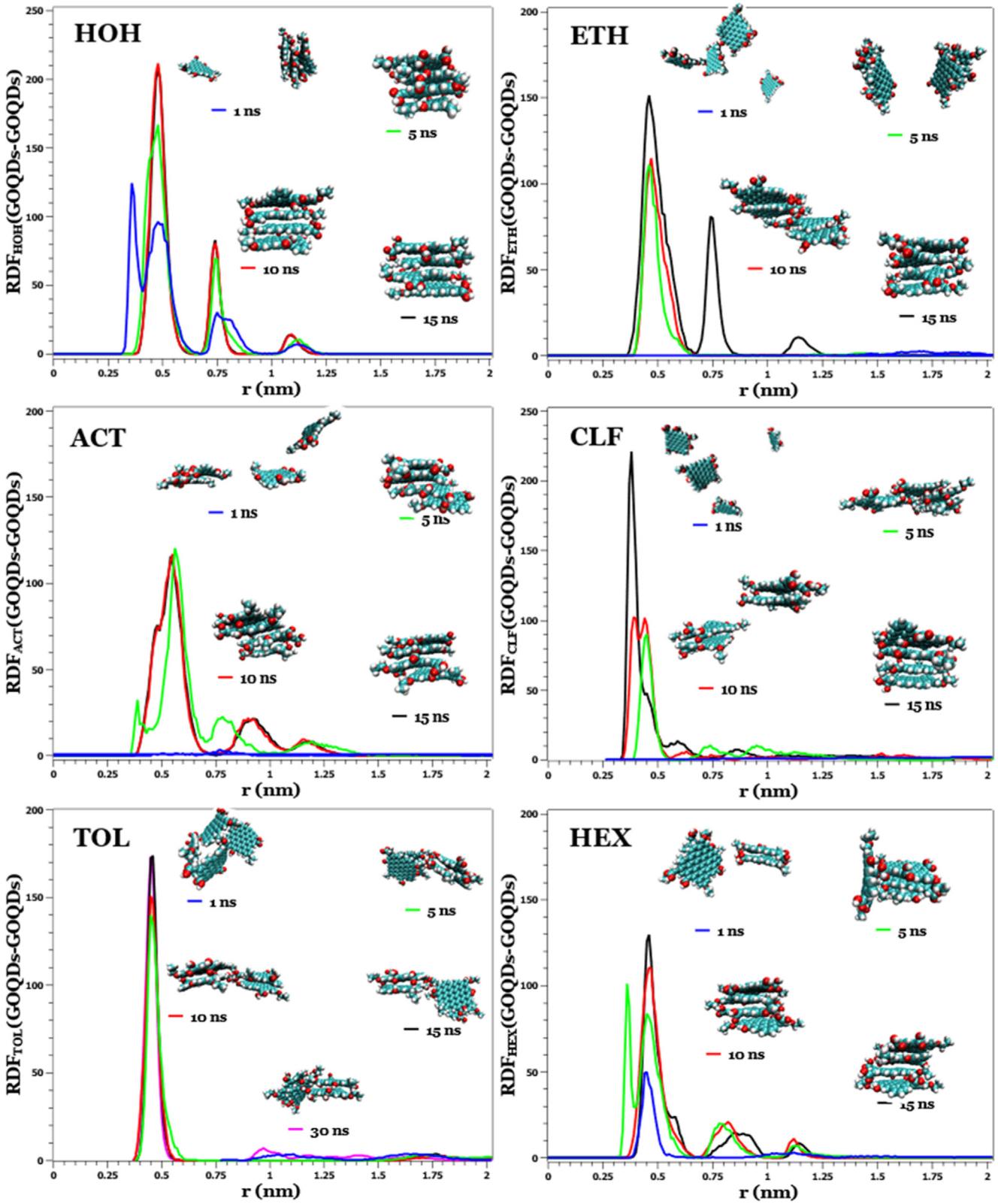

Fig. 6. RDF curves of GOQDs-GOQDS in different solvents after 1, 5, 10, and 15 ns (30 ns for toluene). Snapshots of GOQDs aggregation state after 1, 5, 10, and 15 ns are displayed in the inset.

well-defined absorption bands: B1 (core band, between 200 and 250 nm) caused by the $\pi \rightarrow \pi^*$ electronic transition of the C=C bonds in the aromatic structure, B2 (edge band, between 300 and 400 nm) corresponding to the $n \rightarrow \pi^*$ electronic transitions related to the C=O bonds, and B3 (surface band, with low energy absorption >400 nm) assigned to the surface state of GOQDs. These elec-

tronic transitions are characteristic of graphenic materials with a certain oxidation degree (—OH and —COOH), as proposed in this study [12,13,38,55,56].

However, these theoretical results are not replicated experimentally when the GOQDs are studied in different solvents. Experimental UV–Vis spectroscopy shows that the local solvent structure around GOQDs changes their optical properties (red and blue shifting, and shape variation of the experimental absorption spectra) [57,58]. As observed in Fig. 3, the measured absorption varies towards greater or lesser wavelengths (bathochromic or hypsochromic, respectively). This variation is due to the GOQDs-solvent interaction and the electronic effect of the solvent [33,58]. In non-polar solvents, the negative solvatochromism provokes a hypsochromic shift in the absorption spectra of GOQDs [22]. In oxygenated, non-polar, aromatic compounds, this behavior associates with two phenomena: (1) the effect of the chemical structure of solvent molecules around GOQDs particles (solute–solvent interaction) and (2) the formation of H-type GOQDs aggregates (face-to-face configuration) that causes a blueshift in carbonic structures [58,59].

The experimental absorption spectra show a redshift tendency for GOQDs in less polar solvents than water (Fig. 3 and Fig. S2). In acetone, the oxygen of the carbonyl group (C═O), a typical Lewis base, has a small π-π interaction with the oxygenated groups of the GOQDs [60]. This is possible due to the preferable parallel orientation between the acetone and the GOQDs [61]. The redshift of the spectra in toluene results from the strong π-π interaction between the solvent molecules and the GOQDs [58]. Finally, n-hexane and chloroform molecules interact with GOQDs particles through Van der Waals forces because of their nature. In water, ethanol, and acetone, they do it through hydrogen bond interactions [58].

3.2. Local structure of solvent around GOQDs particles

To understand the previously observed effect of solvents of different nature and polarity on the behavior of GOQDs, a molecular dynamics (MD) study was carried out. These solvents can be categorized into protic polar (water, ethanol), aprotic polar (acetone), non-polar (chloroform, n-hexane), and aromatic (toluene) [58]. During the simulation, the distance between representative sites of these solvent molecules (center of mass, oxygen, hydrogen, or specific carbon atoms) and of the GOQDs (center of mass and oxygen atom) was evaluated. The analysis of these distances through the construction of RDF curves allowed the determination of the solvent molecular behavior around GOQDs in an instant (5 ns). Our results suggest that, during the simulation, the behavior of solvent molecules around GOQDs does not change. The peak intensity variations observed in the RDF curves are only related to the GOQDs aggregation.

First, the RDF curves between the center of masses of GOQDs and solvent molecules (COM-COM) were analyzed. These curves give information about the organization of solvent molecules due to their interaction with the surface of GOQDs (Fig. 4, black lines). The COM-COM RDF curves of GOQDs in water and acetone present a broad curve with no peaks. This indicates a small association between the solvent molecules and the surface of GOQDs [32]. On the other hand, RDF curves of GOQDs in ethanol, chloroform, toluene, and n-hexane show the appearance of an intense peak. This suggests a greater organization of the solvent molecules around GOQDs.

Second, RDF curves between GOQDs COM and the oxygen atoms of the solvents were constructed (red lines in Fig. 4). RDF curves of GOQDs in water, ethanol, and acetone show a small peak

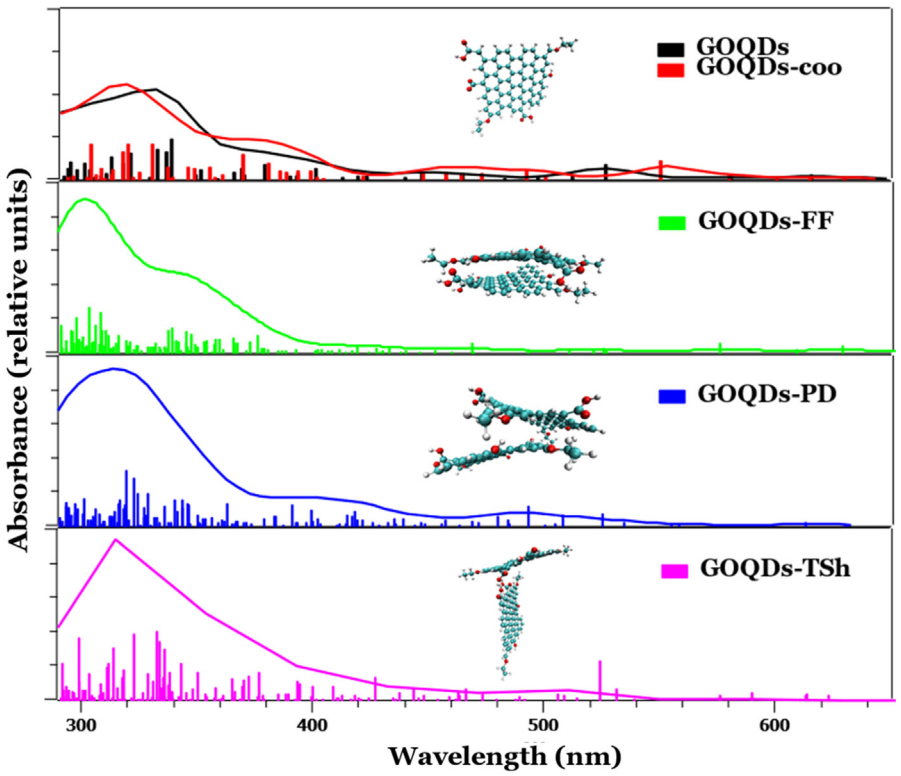

Fig. 7. Calculated absorption spectra of different configurations adopted by GOQDs: face-to-face (FF), parallel displaced (PD), T-shaped (TSh), and deprotonated COOH in GOQDs (coo). The intensity of the UV–Vis spectra peaks of isolated GOQDs (black) and GOQDs-coo have been duplicated for a better analysis.

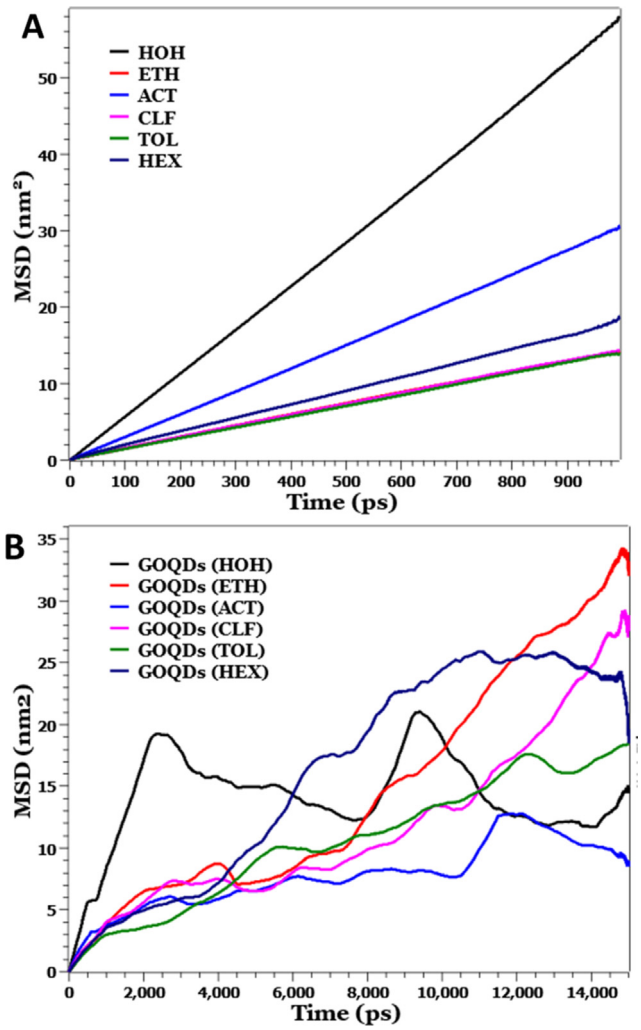

Fig. 8. (A) MSD of solvents (water, ethanol, acetone, chloroform, toluene, and n-hexane) and (B) MSD of GOQDs during the aggregation process.

at 0.18 nm, indicating the preferential orientation of the solvent atoms around the carbon atoms of GOQDs. In contrast, the broad curve with no peaks of the RDF curve of GOQDs in chloroform suggests the absence of preferred orientation. In toluene and n-hexane, the observed wide peak at 0.5 nm indicates that these solvents molecules have a preferred orientation parallel to the GOQDs. The main intermolecular forces present in the interaction between GOQDs and these solvents are weak Van der Waals [30,58] and strong π-π stacking, respectively. GOQDs in toluene present an additional interaction between the oxygenated groups of GOQDs and the solvent (OH— π interactions), which causes the shifting observed in the UV–Vis spectra (Fig. 5C) [58].

Finally, interactions between the oxygenated groups in the GOQDs and the oxygen atoms of the solvents were evaluated (blue lines in Fig. 4). RDF curves of GOQDs in water, ethanol, and acetone present a peak at ~0.28 nm. This indicates the formation of hydrogen bonds between GOQDs and these solvents, as shown in Fig. 5A, B, and C [62,63]. In particular, ethanol molecules present a much more organized structure around the oxygenated groups of the GOQDs, specifically, around the ethoxy groups of the GOQDs (Fig. 5B).

3.3. Aggregation mechanism of GOQDs

To understand the influence of the solvents on the size and formation rate of GOQDs aggregates, we performed an MD simulation for every solvent. Fig. 6 displays snapshots of the aggregated structures of GOQDs and the COM-COM RDF curves between GOQDs in each solvent over time. Overall, the presence of peaks at ~0.75 nm indicates that GOQDs exhibit a moderate to high tendency to aggregate in water (<1 ns), n-hexane and acetone (<10 ns), and ethanol (<15 ns). In contrast, GOQDs in chloroform and toluene show a decreasing tendency to aggregation.

According to the RDF curves, the aggregation of GOQDs in water begins instantaneously due to the π-π interaction of the uncharged GOQDs, reaching a separation distance of ~0.36 nm (COM-COM). This distance is similar to the observed separation between graphene sheets and carbon dots without oxygenated functional groups [27,29,31]. Once this distance is reached, the repulsion between the functional groups in GOQDs rotates the sheets until a stable separation of ~0.47 nm is reached, with no further distancing between aggregated GOQDs [27], In contrast, the RDF curves of GOQDs in ethanol show that the aggregation of GOQDs begins only after 10 ns. RDF curves of GOQDs in n-hexane and acetone display small peaks, which indicates the formation of aggregates with different configurations. In acetone, the peaks at ~0.55 nm and ~0.9 nm indicate a significant separation between the GOQD layers and greater stacking order of the GOQDs layers, respectively. RDF curves of GOQDS in chloroform and toluene, show only a peak at ~0.4 nm, indicating a low aggregation degree of GOQDs.

The adopted structure of GOQDs aggregates and their aggregation mechanism can be determined from the snapshots and RDF curves of Fig. 6. These adopted configurations can be face-to-face, T-shaped, or parallel-displaced. In the face-to-face structure, the π-π interactions of the aromatic particles are optimized, and the separation distance between GOQDs sheets is the minimum [36]. The parallel-displaced and T-shaped configurations present a greater separation between GOQDs and depend on the size [32], the structure of the GOQDs [32,35], and the structure and composition of the solvent molecules [32]. GOQDs in water quickly adopt a face-to-face configuration; in ethanol, the aggregates of GOQDs initially form a parallel displaced configuration before adopting a fully stacked structure. In acetone, a parallel-displaced structure is observed. In n-hexane, the GOQDs aggregates adopt a T-shaped configuration formation. In chloroform and toluene, the appearance of dimers is observed, showing less tendency to aggregate.

These aggregation configurations adopted by the GOQDs in every solvent can be related to the observed optical behavior shown in Fig. 3. To achieve this, the absorption spectra of GOQDs were calculated using the density functional theory and the CAM-B3LYP/6-31G(d) level of theory. Results show that face-to-face, parallel-displaced, and T-shaped configurations change the spectra obtained for isolated GOQDs (Fig. 7). The face-to-face configuration shows a blueshift. On the other hand, the parallel-displaced and T-shape configurations show a redshift of the spectra. Furthermore, OH-π interactions between the GOQDs aggregated in a T-shape configuration in n-hexane produce a change in the shape of the calculated absorption spectrum [58]. A redshifting of the absorption spectra is also observed when GOQDs are deprotonated, as occurs in an environment such as acetone.

3.4. Interactions involved in the aggregation mechanism of GOQDs

The mean square displacement (MSD) was calculated to understand the mobility of the solvent molecules (Fig. 8A) [64]. The results indicate that the mobility of solvent molecules decreases according to water > acetone > n-hexane > chloroform > toluene = ethanol. The similar mobility of ethanol and toluene relates to intermolecular interactions of hydrogen bonding and π-π stacking between the solvent molecules, respectively. The species with the highest diffusion rate (water, acetone, and n-hexane) are those in

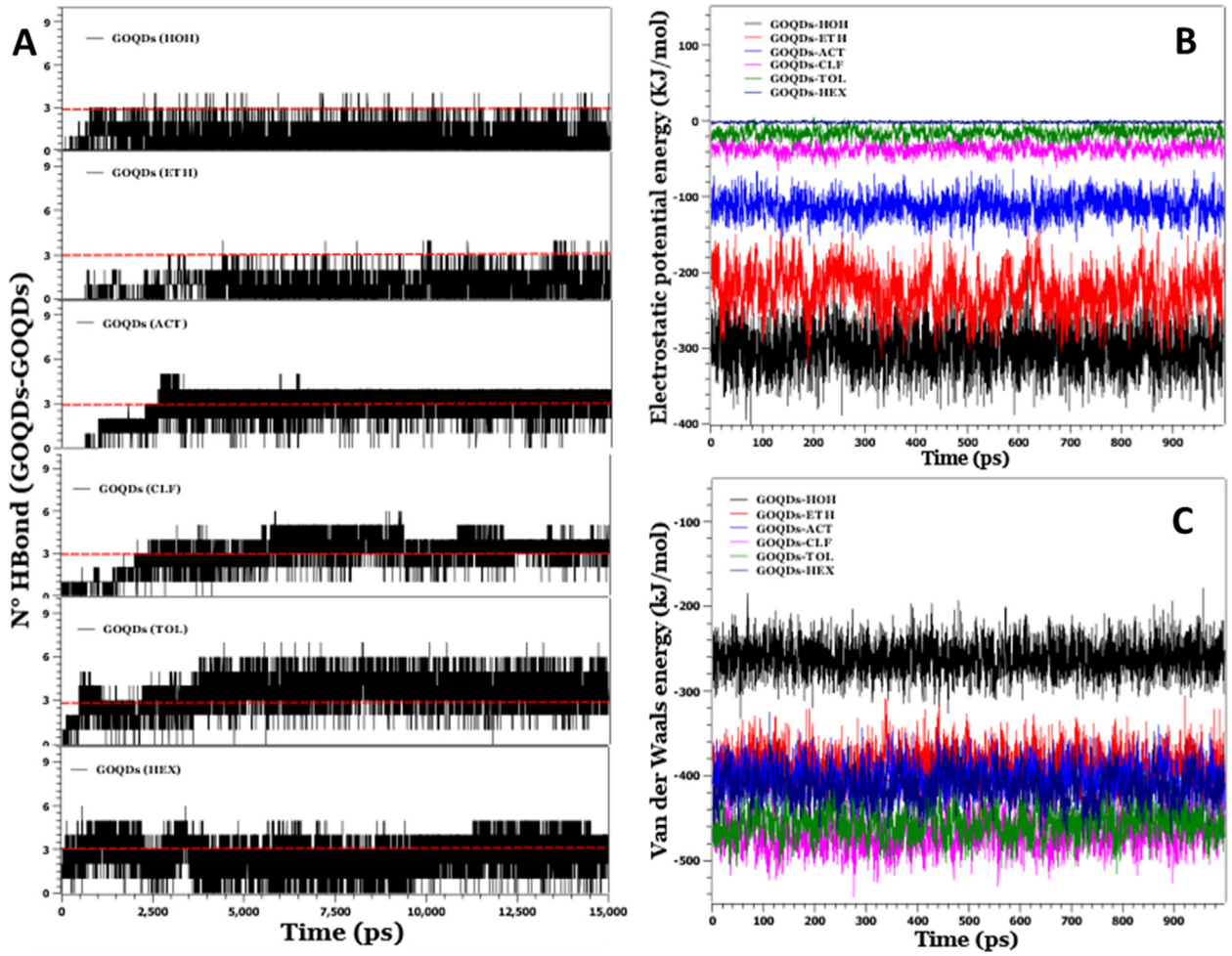

Fig. 9. (A) Number of intermolecular H-bond interactions among GOQDs. (B) Electrostatic and (C) van der Waals energies between GOQDs and solvent molecules.

which GOQDs have a high aggregation degree [30] (Fig. 6). In contrast, solvents with the lowest diffusion rate (chloroform, toluene, and ethanol during the initial instants) show a low aggregation degree. These results show the importance of solvent collision processes during the GOQDs aggregation in different media [29]. RDF curves made for solvents bulk (Fig. S4) show good agreement with the literature, and for small molecules like water, acetone, and chloroform, these show the presence of compact solvation spheres [65–69].

These MSD curves were also calculated to illustrate GOQDs aggregation dynamics in different solvents (Fig. 8B). The observed steep curve of GOQDs in water indicates that GOQDs move freely, while the flat curves in the acetone and toluene solvents indicate that the GOQDs move slowly in these [70]. This movement restriction of GOQDs in toluene is caused by the strong π-π interactions between them. In ethanol, the hydrogen bonds between ethanol molecules (—OH) and GOQDs particles (—OH and —COOH) [71], and the interaction between the alkyl chains in both ethanol and GOQDs, allow the formation of a solvent layer around the GOQDs at the beginning (Fig. 4). This layer reduces the mobility of GOQDs in ethanol. MSD curves show a decrease in the diffusion rate of GOQD particles in all solvents, especially in water. This phenomenon is caused by the GOQDs aggregation, which must move with the rest of the aggregated GOQDs and the recently formed coordination spheres of the solvent.

Hydrogen bonds (H—bonds) between GOQDs are among the main forces involved in the aggregation mechanism, affecting this phenomenon significantly [29]. Fig. 9.A displays the number of H-bonds formed between GOQDs over time in each solvent. In this figure, a more significant number of these bonds is observed at the beginning of the GOQDs aggregation in n-hexane, followed by toluene and chloroform. These interactions are initially not shown in water, ethanol, and acetone, because these H-bonds only form between the solvent molecules and the GOQDs. This H-bonding between GOQDs and the solvent is only possible in these solvents (Fig. S5). The decrease in the number of H-bond in these solvents is caused by the H-bond formation between GOQDs, which is faster in water, followed by ethanol and, finally, acetone.

Non-bonding, electrostatic, and Van der Waals interactions between GOQDs and the solvent molecules were evaluated to determine their influence on the aggregation process. Fig. 9B shows that the electrostatic energy between the solvents and the GOQDs decreases according to water > ethanol > acetone > chloroform > toluene > n-hexane. This energy is influenced by the oxygen atoms, which have a high polarity and are present in solvents and GOQDs sheets [72]. On the other hand, van der Waals energies are mainly related to the size of the solvent molecule [72], and their effect on GOQDs decrease according to toluene > chloroform > n-hexane > acetone > ethanol > water. This interaction contributes to the low tendency to form aggregates, which was found for toluene and chloroform.

According to the obtained results, the GOQDs aggregation mechanism is driven by different forces and π-π stacking interactions. In water, H-bonds and the collision between water

molecules are the main forces that drive the aggregation phenomena [29]. In ethanol, the solvent molecules form coordination spheres based on van der Waals interactions (non-polar side) and H-bonds (polar side) that restrict the movement of GOQDs and, at the same time, the solvent. For its part, acetone molecules interact through H-bonds and act as a Lewis base in the presence of GOQDs, decreasing the mobility of GOQDs. Chloroform molecules interact with GOQDs and other solvent molecules by van der Waals interactions. Toluene molecules create a strong π-π stacking interaction between solvent molecules and between solvent and GOQDs, restricting their mobility and aggregation. In n-hexane, the molecules form a horizontal layer of solvent on the surface of the GOQDs. The displacement of this solvent layer by other sheets of GOQDs during the aggregation [30], generates a T-shaped aggregation configuration. These results suggest that GOQDs have a better dispersion in toluene and chloroform and that GOQDs form a stable dispersion, compared to GOQDs in water [3,40].

4. Conclusions

GOQDs were synthesized by a simple, fast, highly scalable, and environmentally friendly electrochemical carbonization method. FT-IR spectroscopy was used for the characterization of this material. The optical properties of these molecules in different solvents were analyzed by UV–Vis spectroscopy, finding an effect of the solvent on the aggregation state and these properties.

To study the behavior of GOQDs in different solvents, MD methods were used. These simulations were carried out using solvents of different nature, such as polar (water, ethanol, and acetone), non-polar (chloroform and n-hexane), and aromatic (toluene). RDF curves constructed from these simulations were analyzed to understand the nature of the interactions between solvent molecules and GOQDs. These results showed a greater tendency to GOQDs aggregation in water, n-hexane, acetone, and ethanol and a higher degree of stabilization in chloroform and toluene. The optical behavior and the aggregation mechanism of GOQDs in different solvents depend on their interaction with the solvent, the interaction with themselves, and the collision between the solvent molecules. The dominant forces that accompany the π-π interactions during the aggregation of GOQDs vary in different solvents. In water predominates the collision of solvent molecules and hydrogen bonds. In ethanol, hydrogen bonds and van der Waals are the main forces. In acetone, a Lewis base that causes a redshift in absorption spectra, the dominant forces are hydrogen bonds. GOQDs in chloroform only are affected by van der Waals interactions. In toluene, it dominates the π-π interactions with solvent molecules, which affects the absorption spectra due to the OH—π interaction. In n-hexane, the dominant forces are the solvent molecules collision, van der Waals interactions, and hydrogen bonds among the GOQDs. In this solvent, the OH-π interaction between GOQDs is also observed, which changes their absorption spectra. The final geometry of the GOQDs aggregates was determined by the analysis of RDF curves. Results indicate that the aggregation of GOQDs is face-to-face in water and ethanol and parallel displaced in acetone and n-hexane. In contrast, in chloroform and toluene, a low degree of aggregation is observed. This behavior of GOQDs in chloroform and toluene indicates that these solvents can be used to purify GOQDs by solvent extraction and prepare composites.

CRediT authorship contribution statement

V.R. Jauja-Ccana: Conceptualization, Visualization, Methodology, Investigation, Writing - original draft, Writing - review & editing, Software, Formal analysis, Validation. **Allison V. Cordova Huaman:** Visualization, Methodology, Investigation, Formal analysis, Writing - review & editing. **Gustavo T. Feliciano:** Conceptualization, Writing - review & editing, Supervision, Software, Validation. **Adolfo La Rosa Toro:** Conceptualization, Resources, Visualization, Writing - review & editing, Supervision, Validation.

Declaration of Competing Interest

The authors declare that they have no known competing financial interests or personal relationships that could have appeared to influence the work reported in this paper.

Acknowledgments

This work was financially supported by the Fondo Nacional de Desarrollo Científico, Tecnológico y de Innovación Tecnológica of Peru (CONV-000208-2015-FONDECYT-DE). The authors thank to the Laboratory Investigation of Biopolymers and Metallopharmaceuticals (LIBIPMET) for the computational resources.

Appendix A. Supplementary material

Supplementary data to this article can be found online at https://doi.org/10.1016/j.molliq.2021.116136.

References

[1] G. Rajender, J. Kumar, P.K. Giri, Interfacial charge transfer in oxygen deficient TiO2-graphene quantum dot hybrid and its influence on the enhanced visible light photocatalysis, Appl. Catal. B Environ. 224 (2018) 960–972, https://doi.org/10.1016/j.apcatb.2017.11.042.
[2] H. Jin, H. Huang, Y. He, X. Feng, S. Wang, L. Dai, J. Wang, Graphene quantum dots supported by graphene nanoribbons with ultrahigh electrocatalytic performance for oxygen reduction, J. Am. Chem. Soc. 137 (2015) 7588–7591, https://doi.org/10.1021/jacs.5b03799.
[3] M.K. Kumawat, M. Thakur, R.B. Gurung, R. Srivastava, Graphene quantum dots from *mangifera indica*: application in near-infrared bioimaging and intracellular nanothermometry, ACS Sustain. Chem. Eng. 5 (2017) 1382–1391, https://doi.org/10.1021/acssuschemeng.6b01893.
[4] S.L. Ting, S.J. Ee, A. Ananthanarayanan, K.C. Leong, P. Chen, Graphene quantum dots functionalized gold nanoparticles for sensitive electrochemical detection of heavy metal ions, Electrochim. Acta. 172 (2015) 7–11, https://doi.org/10.1016/j.electacta.2015.01.026.
[5] T.C. Canevari, M. Nakamura, F.H. Cincotto, F.M. De Melo, H.E. Toma, High performance electrochemical sensors for dopamine and epinephrine using nanocrystalline carbon quantum dots obtained under controlled chronoamperometric conditions, Electrochim. Acta. 209 (2016) 464–470, https://doi.org/10.1016/j.electacta.2016.05.108.
[6] B.J. Moon, K.S. Lee, J. Shim, S. Park, S.H. Kim, S. Bae, M. Park, C.L. Lee, W.K. Choi, Y. Yi, J.Y. Hwang, D.I. Son, Enhanced photovoltaic performance of inverted polymer solar cells utilizing versatile chemically functionalized ZnO@graphene quantum dot monolayer, Nano Energy 20 (2016) 221–232, https://doi.org/10.1016/j.nanoen.2015.11.039.
[7] X. Zhao, W. Gao, H. Zhang, X. Qiu, Y. Luo, Graphene quantum dots in biomedical applications: recent advances and future challenges, Handb. Nanomater. Anal. Chem. (2020) 493–505, https://doi.org/10.1016/B978-0-12-816699-4.00020-7, Elsevier.
[8] T. Fan, W. Zeng, W. Tang, C. Yuan, S. Tong, K. Cai, Y. Liu, W. Huang, Y. Min, A.J. Epstein, Controllable size-selective method to prepare graphene quantum dots from graphene oxide, Nanoscale Res. Lett. 10 (2015), https://doi.org/10.1186/s11671-015-0783-9.
[9] M. He, X. Guo, J. Huang, H. Shen, Q. Zeng, L. Wang, Mass production of tunable multicolor graphene quantum dots from an energy resource of coke by a one-step electrochemical exfoliation, Carbon N. Y. 140 (2018) 508–520, https://doi.org/10.1016/j.carbon.2018.08.067.
[10] L. Zhu, Q. Yue, D. Jiang, H. Chen, R.M. Irfan, P. Du, Metal-free graphene quantum dots photosensitizer coupled with nickel phosphide cocatalyst for enhanced photocatalytic hydrogen production in water under visible light, Cuihua Xuebao/Chinese J. Catal. 39 (2018) 1753–1761, https://doi.org/10.1016/S1872-2067(18)63135-3.
[11] X. Yan, X. Cui, L. Li, Synthesis of large, stable colloidal graphene quantum dots with tunable size, J. Am. Chem. Soc. 132 (2010) 5944–5945, https://doi.org/10.1021/ja1009376.
[12] M.H. Jang, H. Yang, Y.H. Chang, H.C. Park, H. Park, H.H. Cho, B.J. Kim, Y.H. Kim, Y.H. Cho, Selective engineering of oxygen-containing functional groups using the alkyl ligand oleylamine for revealing the luminescence mechanism of

graphene oxide quantum dots, Nanoscale 9 (2017) 18635–18643, https://doi.org/10.1039/c7nr04150k.
[13] S. Ahirwar, S. Mallick, D. Bahadur, Electrochemical method to prepare graphene quantum dots and graphene oxide quantum dots, ACS Omega 2 (2017) 8343–8353, https://doi.org/10.1021/acsomega.7b01539.
[14] V. Sharma, P.K. Jha, Enhancement in power conversion efficiency of edge-functionalized graphene quantum dot through adatoms for solar cell applications, Sol. Energy Mater. Sol. Cells. 200 (2019), https://doi.org/10.1016/j.solmat.2019.04.030.
[15] S. Jeong, R.L. Pinals, B. Dharmadhikari, H. Song, A. Kalluri, D. Debnath, Q. Wu, M.H. Ham, P. Patra, M.P. Landry, Graphene quantum dot oxidation governs noncovalent biopolymer adsorption, Sci. Rep. 10 (2020) 1–14, https://doi.org/10.1038/s41598-020-63769-z.
[16] D. Qu, Z. Sun, M. Zheng, J. Li, Y. Zhang, G. Zhang, H. Zhao, X. Liu, Z. Xie, Three colors emission from S, N Co-doped graphene quantum dots for visible light H_2 production and bioimaging, Adv. Opt. Mater. 3 (2015) 360–367, https://doi.org/10.1002/adom.201400549.
[17] S. Yang, J. Sun, P. He, X. Deng, Z. Wang, C. Hu, G. Ding, X. Xie, Selenium doped graphene quantum dots as an ultrasensitive redox fluorescent switch, Chem. Mater. 27 (2015) 2004–2011, https://doi.org/10.1021/acs.chemmater.5b00112.
[18] S. Ge, J. He, C. Ma, J. Liu, F. Xi, X. Dong, One-step synthesis of boron-doped graphene quantum dots for fluorescent sensors and biosensor, Talanta 199 (2019) 581–589, https://doi.org/10.1016/j.talanta.2019.02.098.
[19] A. Mikhraliieva, V. Zaitsev, O. Tkachenko, M. Nazarkovsky, Y. Xing, E.V. Benvenutti, Graphene oxide quantum dots immobilized on mesoporous silica: preparation, characterization and electroanalytical application, RSC Adv. 10 (2020) 31305–31315, https://doi.org/10.1039/d0ra04605a.
[20] B. Wang, P. Zhao, J. Feng, D. Chen, Y. Huang, L. Sui, H. Dong, S. Ma, L. Dong, L. Yu, Carbon-based 0D/1D/2D assembly with desired structures and defect states as non-metal bifunctional electrocatalyst for zinc-air battery, J. Colloid Interface Sci. 588 (2021) 184–195, https://doi.org/10.1016/j.jcis.2020.12.051.
[21] S. Kang, K.M. Kim, K. jung, Y. Son, S. Mhin, J.H. Ryu, K.B. Shim, B. Lee, H.S. Han, T. Song, Graphene oxide quantum dots derived from coal for bioimaging facile and green approach, Sci. Rep. 9 (2019) 1–7, https://doi.org/10.1038/s41598-018-37479-6.
[22] S.J. Bradley, R. Kroon, G. Laufersky, M. Röding, R.V. Goreham, T. Gschneidtner, K. Schroeder, K. Moth-Poulsen, M. Andersson, T. Nann, Heterogeneity in the fluorescence of graphene and graphene oxide quantum dots, Microchim. Acta. 184 (2017) 871–878, https://doi.org/10.1007/s00604-017-2075-9.
[23] A. Cayuela, M.L. Soriano, C. Carrillo-Carrión, M. Valcárcel, Semiconductor and carbon-based fluorescent nanodots: The need for consistency, Chem. Commun. 52 (2016) 1311–1326, https://doi.org/10.1039/c5cc07754k.
[24] S. Chinnusamy, R. Kaur, A. Bokare, F. Erogbogbo, Incorporation of graphene quantum dots to enhance photocatalytic properties of anatase TiO2, MRS Commun. 8 (2018) 137–144, https://doi.org/10.1557/mrc.2018.7.
[25] Q. Li, B. Chen, B. Xing, Aggregation kinetics and self-assembly mechanisms of graphene quantum dots in aqueous solutions: cooperative effects of pH and electrolytes, Environ. Sci. Technol. 51 (2017) 1364–1376, https://doi.org/10.1021/acs.est.6b04178.
[26] S. Min, J. Hou, Y. Lei, X. Ma, G. Lu, Facile one-step hydrothermal synthesis toward strongly coupled TiO_2/graphene quantum dots photocatalysts for efficient hydrogen evolution, Appl. Surf. Sci. 396 (2017) 1375–1382, https://doi.org/10.1016/j.apsusc.2016.11.169.
[27] M. Paloncýová, M. Langer, M. Otyepka, structural dynamics of carbon dots in water and *N*, *N* -dimethylformamide probed by all-atom molecular dynamics simulations, J. Chem. Theory Comput. 14 (2018) 2076–2083, https://doi.org/10.1021/acs.jctc.7b01149.
[28] G.S. Das, J.P. Shim, A. Bhatnagar, K.M. Tripathi, T.Y. Kim, biomass-derived carbon quantum dots for visible-light-induced photocatalysis and label-free detection of Fe(III) and ascorbic acid, Sci. Rep. 9 (2019) 1–9, https://doi.org/10.1038/s41598-019-49266-y.
[29] H. Tang, D. Liu, Y. Zhao, X. Yang, J. Lu, F. Cui, Molecular dynamics study of the aggregation process of graphene oxide in water, J. Phys. Chem. C. 119 (2015) 26712–26718, https://doi.org/10.1021/acs.jpcc.5b07345.
[30] S. Chen, S. Sun, C. Li, C.U. Pittman, T.E. Lacy, S. Hu, S.R. Gwaltney, Molecular dynamics simulations of the aggregation behaviour of overlapped graphene sheets in linear aliphatic hydrocarbons, Mol. Simul. 44 (2018) 947–953, https://doi.org/10.1080/08927022.2018.1465569.
[31] J.H. Cha, W. Kyoung, K. Song, S. Park, T. Lim, J. Lee, H. Kang, Quantitative evaluation of the dispersion of graphene sheets with and without functional groups using molecular dynamics simulations, Nanoscale Res. Lett. 11 (2016), https://doi.org/10.1186/s11671-016-1336-6.
[32] S. Banerjee, Molecular dynamics study of self-agglomeration of charged fullerenes in solvents, J. Chem. Phys. 138 (2013), https://doi.org/10.1063/1.4789304.
[33] T. Malaspina, E.E. Fileti, R. Rivelino, Structure and UV−Vis spectrum of C_{60} fullerene in ethanol: a sequential molecular dynamics/quantum mechanics study, J. Phys. Chem. B. 111 (2007) 11935–11939, https://doi.org/10.1021/jp0746244.
[34] N.R. Tummala, A. Striolo, SDS surfactants on carbon nanotubes: aggregate morphology, ACS Nano 3 (2009) 595–602, https://doi.org/10.1021/nn8007756.
[35] J.L.L.F.S. Costa, D. Simionesie, Z.J. Zhang, P.A. Mulheran, Aggregation of model asphaltenes: a molecular dynamics study, J. Phys. Condens. Matter. 394002 (n. d.) 394002. https://doi.org/10.1088/0953-8984/28/39/394002.
[36] S. Yaseen, G.A. Mansoori, Asphaltene aggregation due to waterflooding (A molecular dynamics study), J. Pet. Sci. Eng. 170 (2018) 177–183, https://doi.org/10.1016/j.petrol.2018.06.043.
[37] N.J. Hestand, F.C. Spano, Expanded theory of H- and J-molecular aggregates: the effects of vibronic coupling and intermolecular charge transfer, Chem. Rev. 118 (2018) 7069–7163, https://doi.org/10.1021/acs.chemrev.7b00581.
[38] T. Ghosh, E. Prasad, White-light emission from unmodified graphene oxide quantum dots, J. Phys. Chem. C. 119 (2015) 2733–2742, https://doi.org/10.1021/jp511787a.
[39] J. Deng, Q. Lu, N. Mi, H. Li, M. Liu, M. Xu, L. Tan, Q. Xie, Y. Zhang, S. Yao, Electrochemical synthesis of carbon nanodots directly from alcohols, Chem. - A Eur. J. 20 (2014) 4993–4999, https://doi.org/10.1002/chem.201304869.
[40] Z.M. Markovic, B.Z. Ristic, K.M. Arsikin, D.G. Klisic, L.M. Harhaji-Trajkovic, B.M. Todorovic-Markovic, D.P. Kepic, T.K. Kravic-Stevovic, S.P. Jovanovic, M.M. Milenkovic, D.D. Milivojevic, V.Z. Bumbasirevic, M.D. Dramicanin, V.S. Trajkovic, Graphene quantum dots as autophagy-inducing photodynamic agents, Biomaterials 33 (2012) 7084–7092, https://doi.org/10.1016/j.biomaterials.2012.06.060.
[41] J. Liu, P. Li, H. Xiao, Y. Zhang, X. Shi, X. Lü, X. Chen, Understanding flocculation mechanism of graphene oxide for organic dyes from water: Experimental and molecular dynamics simulation, AIP Adv. 5 (2015), https://doi.org/10.1063/1.4936846.
[42] L. Wang, B. Wu, W. Li, Z. Li, J. Zhan, B. Geng, S. Wang, D. Pan, M. Wu, Industrial production of ultra-stable sulfonated graphene quantum dots for Golgi apparatus imaging, J. Mater. Chem. B. 5 (2017) 5355–5361, https://doi.org/10.1039/c7tb01348e.
[43] N. Thongsai, P. Jaiyong, S. Kladsomboon, I. In, P. Paoprasert, Utilization of carbon dots from jackfruit for real-time sensing of acetone vapor and understanding the electronic and interfacial interactions using density functional theory, Appl. Surf. Sci. 487 (2019) 1233–1244, https://doi.org/10.1016/j.apsusc.2019.04.269.
[44] J.A., J.E.P., F.O., M.J.B., J.J.H., E.N.B., K.N.K., V.N.S., T.A.K., R.K., J.N., K.R., A.P.R., J.C. B., S.S.I., J.M.J. Frisch, G.W. Trucks, H.B. Schlegel, G.E. Scuseria, M.A. Robb, J.R. Cheeseman, G. Scalmani, V. Barone, G.A. Petersson, H. Nakatsuji, X. Li, M. Caricato, A.V. Marenich, J. Bloino, B.G. Janesko, R.G., Gaussian 16, https://gaussian.com/citation/ (accessed November 5, 2019) (2016).
[45] T. Lu, F. Chen, Multiwfn: A multifunctional wavefunction analyzer, J. Comput. Chem. 33 (2012) 580–592, https://doi.org/10.1002/jcc.22885.
[46] W.L. Jorgensen, D.S. Maxwell, J. Tirado-Rives, Development and testing of the OPLS all-atom force field on conformational energetics and properties of organic liquids, J. Am. Chem. Soc. 118 (1996) 11225–11236, https://doi.org/10.1021/ja9621760.
[47] N. Patra, B. Wang, P. Král, Nanodroplet activated and guided folding of graphene nanostructures, Nano Lett. 9 (2009) 3766–3771, https://doi.org/10.1021/nl9019616.
[48] S. Zeng, G. Zhou, J. Guo, F. Zhou, J. Chen, Molecular simulations of conformation change and aggregation of HIV-1 Vpr13-33 on graphene oxide, Sci. Rep. 6 (2016), https://doi.org/10.1038/srep24906.
[49] B. Hess, C. Kutzner, D. van der Spoel, E. Lindahl, GROMACS 4: algorithms for highly efficient, load-balanced, and scalable molecular simulation, J. Chem. Theory Comput. 4 (2008) 435–447, https://doi.org/10.1021/ct700301q.
[50] Gromacs - Gromacs, http://www.gromacs.org/ (accessed November 5, 2019) (n.d.).
[51] W. Humphrey, A. Dalke, K. Schulten, VMD: visual molecular dynamics, J. Mol. Graph. 14 (1996) 33–38, https://doi.org/10.1016/0263-7855(96)00018-5.
[52] N.J. Kuo, Y.S. Chen, C.W. Wu, C.Y. Huang, Y.H. Chan, I.W.P. Chen, One-pot synthesis of hydrophilic and hydrophobic N-doped graphene quantum dots via exfoliating and disintegrating graphite flakes, Sci. Rep. 6 (2016) 1–11, https://doi.org/10.1038/srep30426.
[53] S. Georgitsopoulou, A. Karakassides, V. Georgakilas, Interfacial asymmetric post-functionalization of graphene: amphiphilic graphene derivatives self-assembled to 3D superstructures, Chem. - A Eur. J. 24 (2018) 17356–17360, https://doi.org/10.1002/chem.201804386.
[54] J.-P. Tessonnier, M.A. Barteau, Dispersion of alkyl-chain-functionalized reduced graphene oxide sheets in nonpolar solvents, Langmuir 28 (2012) 6691–6697, https://doi.org/10.1021/la2051614.
[55] G.M.A. Junqueira, J.P.A. Mendonça, A.H. Lima, W.G. Quirino, F. Sato, Enhancement of nonlinear optical properties of graphene oxide-based structures: Push-pull models, RSC Adv. 6 (2016) 94437–94450, https://doi.org/10.1039/c6ra18314j.
[56] G. Yang, C. Wu, X. Luo, X. Liu, Y. Gao, P. Wu, C. Cai, S. Scott, Saavedra, Exploring the emissive states of heteroatom-doped graphene quantum dots, J. Phys. Chem. C. 122 (2018) 6483–6492, https://doi.org/10.1021/acs.jpcc.8b01385.
[57] K. Smail, N. Tchouar, M. Barj, B. Marekha, A. Idrissi, Luteolin organic solvent interactions. A molecular dynamics simulation analysis, J. Mol. Liq. 212 (2015) 503–508, https://doi.org/10.1016/j.molliq.2015.09.043.
[58] D. Zheng, X.A. Yuan, H. Ma, X. Li, X. Wang, Z. Liu, J. Ma, Unexpected solvent effects on the UV/Vis absorption spectra of o-cresol in toluene and benzene: In contrast with non-aromatic solvents, R. Soc. Open Sci. 5 (2018), https://doi.org/10.1098/rsos.171928.
[59] A. Demchenko, Excitons in carbonic nanostructures, C— J. Carbon Res. 5 (2019) 71, https://doi.org/10.3390/c5040071.
[60] D. Pan, J. Zhang, Z. Li, C. Wu, X. Yan, M. Wu, Observation of pH-, solvent-, spin-, and excitation-dependent blue photoluminescence from carbon nanoparticles, Chem. Commun. 46 (2010) 3681–3683, https://doi.org/10.1039/c000114g.

[61] M.D. Ganji, H. Mazaheri, A. Khosravi, Acetone adsorption on pristine and Pt-doped graphene: a first-principles vdW-DF study, Commun. Theor. Phys. 64 (2015) 576–582, https://doi.org/10.1088/0253-6102/64/5/576.
[62] J. Liu, X. He, J.Z.H. Zhang, L.W. Qi, Hydrogen-bond structure dynamics in bulk water: Insights from: Ab initio simulations with coupled cluster theory, Chem. Sci. 9 (2018) 2065–2073, https://doi.org/10.1039/c7sc04205a.
[63] T.L. Fonseca, K. Coutinho, S. Canuto, Hydrogen bond interactions between acetone and supercritical water, Phys. Chem. Chem. Phys. 12 (2010) 6660–6665, https://doi.org/10.1039/b926527a.
[64] K.M. Gupta, Z. Hu, J. Jiang, Cellulose regeneration from a cellulose/ionic liquid mixture: the role of anti-solvents, RSC Adv. 3 (2013) 12794–12801, https://doi.org/10.1039/c3ra40807h.
[65] V. Rühle, C. Junghans, Hybrid approaches to coarse-graining using the VOTCA package: liquid hexane, Macromol. Theory Simul. 20 (2011) 472–477, https://doi.org/10.1002/mats.201100011.
[66] Y. Ding, First principles molecular dynamics investigation on the water-ion interaction: a case of diluted CsI solution, Chem. Phys. Lett. 760 (2020), https://doi.org/10.1016/j.cplett.2020.137996 137996.
[67] F. Moosavi, M. Gholizadeh, Magnetic effects on the solvent properties investigated by molecular dynamics simulation, J. Magn. Magn. Mater. 354 (2014) 239–247, https://doi.org/10.1016/j.jmmm.2013.11.012.
[68] Y.G. Bushuev, S.V. Davletbaeva, Structural properties of liquid acetone, Russ. Chem. Bull. 48 (1999) 25–34, https://doi.org/10.1007/BF02494395.
[69] W. Dietz, K. Heinzinger, A molecular dynamics study of liquid chloroform, Berichte Der Bunsengesellschaft Für Phys, Chemie 89 (1985) 968–977, https://doi.org/10.1002/bbpc.19850890909.
[70] J.-Q. Lin, H.-W. Zhang, Z. Chen, Y.-G. Zheng, Z.-Q. Zhang, H.-F. Ye, Simulation study of aggregations of monolayer-protected gold nanoparticles in solvents, J. Phys. Chem. C. 115 (2011) 18991–18998, https://doi.org/10.1021/jp204735d.
[71] D. Damasceno Borges, C.F. Woellner, P.A.S. Autreto, D.S. Galvao, Insights on the mechanism of water-alcohol separation in multilayer graphene oxide membranes: entropic versus enthalpic factors, Carbon N. Y. 127 (2018) 280–286, https://doi.org/10.1016/j.carbon.2017.11.020.
[72] S. Yaseen, G.A. Mansoori, Molecular dynamics studies of interaction between asphaltenes and solvents, J. Pet. Sci. Eng. 156 (2017) 118–124, https://doi.org/10.1016/j.petrol.2017.05.018.